

Controlling a CyberOctopus Soft Arm with Muscle-like Actuation

Heng-Sheng Chang^{1,2}, Udit Halder², Ekaterina Gribkova³, Arman Tekinalp¹,

Noel Naughton¹, Mattia Gazzola^{1,4,5}, Prashant G. Mehta^{1,2}

Abstract—This paper entails the application of the energy shaping methodology to control a flexible, elastic Cosserat rod model of a single octopus arm. The principal focus and novel contribution of this work is two-fold: (i) reduced order control-oriented modeling of the realistic internal muscular architecture in an octopus arm; and (ii) incorporation of such models into the energy shaping methodology, extending our prior work by formally accounting for muscle constraints. Extension of the control scheme to the under-actuated muscle control case involves two steps: (i) design of a desired potential energy function whose static minimizer solves a given control task; and (ii) implementing the resulting energy shaping control input into the dynamic model. Due to the muscle actuator constraints, the desired potential energy function may not be arbitrarily chosen. Indeed, the desired energy must now satisfy a partial differential equation, known as the matching condition, which is derived for the infinite dimensional Hamiltonian control system. A particular solution to those matching conditions is described, paving the way to the application of energy shaping methodology. The overall control design methodology including muscle models is implemented and demonstrated in a dynamic simulation environment. Results of several bio-inspired numerical experiments involving the control of octopus arms are reported.

Index Terms—Cosserat rod, Hamiltonian systems, energy-shaping control, soft robotics, octopus

I. INTRODUCTION

Research interest in soft robotic manipulators has recently increased manifold. This interest is primarily driven by the potential capability of soft manipulators to perform complex tasks [1]–[3]. There are a number of examples of biological soft-bodied marine creatures, such as octopuses, that have evolved to solve complex motion control problems such as reaching, grasping, fetching, crawling, or swimming. The exceptional coordination abilities of these creatures have naturally motivated an effort to gain a deeper understanding of the biophysical principles underlying their distributed neuromuscular control.

This paper is a continuation of our prior work where an energy shaping methodology was introduced for a fully

actuated Cosserat rod model of an octopus arm. The methodology was applied to solve a number of motion problems, e.g. reaching and grasping, inspired by observed motion patterns in octopus arms. The main limitation was that the muscle actuator constraints were ignored in this prior work. Constraints arise both due to the discrete nature of the muscle groups as well as saturation in the muscle-generated forces and couples. These constraints serve to limit the energy landscape that can possibly be ‘shaped’ by use of control. The mathematical characterization of achievable energy is given in terms of the so called *matching conditions* [4], [5]. However, general solutions to these conditions are not easy to obtain [6], [7].

The contributions of this work are two-fold:

(i) **Development of control-oriented muscle models:** Octopus arms are controlled by the internal musculature whose anatomical structure is well documented [8]–[12]. The octopus muscles are categorized into three groups: longitudinal, transverse, and oblique. In this paper, reduced order models of longitudinal and transverse muscles are developed based on the Hill’s skeletal muscle model [13], [14]. The proposed models are adequately able to capture the generation of forces and torques along specific directions consistent with anatomical studies.

(ii) **Energy shaping using muscle model constraints:** The force and torque profiles for different muscle groups are used to develop the matching conditions for the muscle-controlled arm. A particular solution to these equations is provided. The solution is used to obtain the desired potential energy and the associated control law. The dynamics of the arm together with the muscle actuation model are simulated in the computational platform *Elastica* [15], [16]. The control methodology is implemented and demonstrated for a reaching and a grasping task.

The remainder of this paper is organized as follows: The elements of the planar Cosserat rod theory are briefed in Sec. II. The mathematical muscle model, including an overview of the arm musculature and the Hill’s model, is described in Sec. III. A derivation and solution to the matching conditions are given in Sec. IV. The results of the numerical experiments are reported in Sec. V. The paper is concluded with directions of future research in Sec. VI.

II. A SINGLE ARM MODELED AS A COSSERAT ROD

We consider a Cosserat rod in a plane spanned by the fixed orthonormal basis $\{e_1, e_2\}$. The rod is a one-dimensional continuum deformable object with rest length L_0 . Along

We gratefully acknowledge financial support from ONR MURI N00014-19-1-2373 (G.C., M.G., M.G.P.), NSF/USDA #2019-67021-28989 (G.C., M.G.), and NSF EFRI C3 SoRo #1830881 (M.G.). We also acknowledge computing resources provided by the Blue Waters project (OCI- 0725070, ACI-1238993), a joint effort of the University of Illinois at Urbana-Champaign and its National Center for Supercomputing Applications, and the Extreme Science and Engineering Discovery Environment (XSEDE) Stampede2 (ACI-1548562) at the Texas Advanced Computing Center (TACC) through allocation TG-MCB190004.

¹Department of Mechanical Science and Engineering, ²Coordinated Science Laboratory, ³Neuroscience Program, ⁴National Center for Supercomputing Applications, & ⁵Carl R. Woese Institute for Genomic Biology, University of Illinois at Urbana-Champaign. Corresponding e-mail: udit@illinois.edu

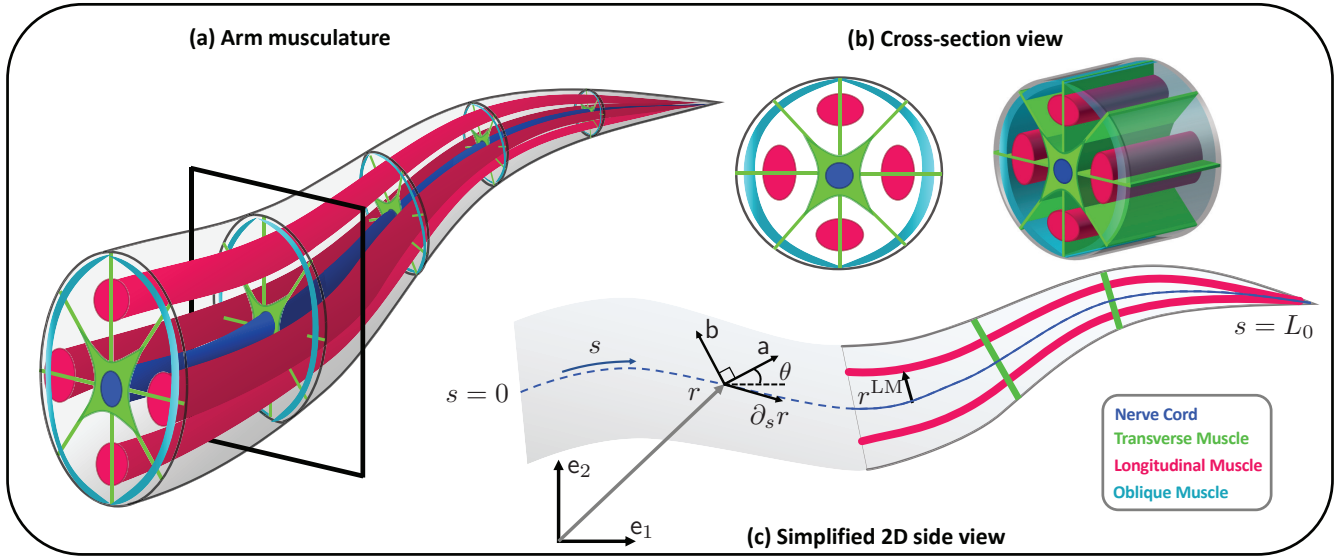


Fig. 1: An octopus arm is modeled as a Cosserat rod – (a) a simplified 3D view of the internal musculature, (b) a cross-section of the arm showing organization of different kinds of muscles, and (c) a 2D model of the arm where we only consider effects of longitudinal and transverse muscles.

with time $t \in \mathbb{R}$, the arc-length parameter $s \in [0, L_0]$ of the center line are the independent coordinates of the rod. The *state* of the rod is described by the function $q(s, t) := (r(s, t), \theta(s, t))$, where $r = (x, y) \in \mathbb{R}^2$ denotes the position vector of the center line, and the angle θ , here considered as a real variable, defines a material frame spanned by the orthonormal basis $\{a, b\}$, where $a = \cos \theta e_1 + \sin \theta e_2$, $b = -\sin \theta e_1 + \cos \theta e_2$ (see Fig. 1c). The deviation of frame $\{a, b\}$ from the pair $\partial_s r$ and its perpendicular vector represents the local stretch and shear strain of the rod, denoted as ν_1 and ν_2 , respectively. The curvature strain κ completes the triad of *strains* or *deformations* $w = (\nu_1, \nu_2, \kappa)$, with the defining relationship

$$\partial_s q = \begin{bmatrix} \partial_s r \\ \partial_s \theta \end{bmatrix} = \begin{bmatrix} \nu_1 a + \nu_2 b \\ \kappa \end{bmatrix} =: f(q, w) \quad (1)$$

A. Statics – potential energy and its shaping

The study of statics of the rod is concerned with finding an equilibrium configuration of the rod, under various external or internal loads. Essential to this process is the introduction of the potential energy function of the rod

$$\mathcal{V}(q) = \int_0^{L_0} W(w(s)) ds \quad (2)$$

where $W : (\nu_1, \nu_2, \kappa) \mapsto \mathbb{R}$ is referred to as the *stored energy function*. For a hyperelastic rod, the internal stresses are found from the partial derivative of W with respect to its arguments [17]. For simplicity, we consider a perfectly elastic rod for which the stress-strain relationship is linear. That is, W is of the quadratic form

$$W = \frac{1}{2} (EA(\nu_1 - \nu_1^\circ)^2 + GA(\nu_2 - \nu_2^\circ)^2 + EI(\kappa - \kappa^\circ)^2)$$

E and G are the material Young's and shear moduli, A and I are the cross sectional area and second moment of area,

and $\nu_1^\circ, \nu_2^\circ, \kappa^\circ$ are the intrinsic strains that determine the rod's shape at rest. If $\nu_1^\circ \equiv 1, \nu_2^\circ \equiv 0, \kappa^\circ \equiv 0$, then the rest configuration is a straight rod of length L_0 .

The problem of finding an equilibrium configuration of the rod is tantamount to finding its equilibrium deformation. Indeed, given a boundary condition and deformations, (1) is integrated to obtain the static equilibrium. In our prior work [18], this motivated the following model of desired potential energy

$$\mathcal{V}^d = \frac{1}{2} \int_0^{L_0} \left(EA(\nu_1 - \nu_1^d)^2 + GA(\nu_2 - \nu_2^d)^2 + EI(\kappa - \kappa^d)^2 \right) ds \quad (3)$$

in terms of – yet to be chosen – desired deformation $w^d = (\nu_1^d, \nu_2^d, \kappa^d)$. Clearly, w^d is the minimizer and the static equilibrium is simply obtained by integrating (1) from a given boundary condition.

It remains to choose the desired deformation. In our prior work, this is done by solving the following optimization problem:

$$\begin{aligned} \underset{w(\cdot)}{\text{minimize}} \quad & J = \int_0^{L_0} W(w(s)) + \mu_{\text{grasp}}(s) \Phi_{\text{grasp}}(q(s)) ds \\ & + \mu_{\text{tip}} \Phi_{\text{tip}}(q(L_0), q^*) \\ \text{subject to} \quad & \partial_s q = f(q, w), \quad \text{with } q(0) = q_0, \quad q(L_0) \text{ free;} \\ & \text{and } \Psi_j(q) \leq 0, \quad j = 1, 2, \dots, N_{\text{obs}} \end{aligned} \quad (4)$$

The problem represents a modification of the intrinsic potential energy of the rod to include additional control task specific terms: the terminal cost function Φ_{tip} penalizes the distance between the arm tip and a given target $q^* \in \mathbb{R}^3$, Φ_{grasp} is chosen to achieve a grasping task, parameters

μ_{tip} and μ_{grasp} are designed according to the objective, the inequalities $\Psi_j < 0$ represent obstacles in the environment (see [18] for more details including several bio-inspired examples).

B. Dynamics – a Hamiltonian control system

The momentum $p := M\partial_t q$, together with the state q , completely describe the spatio-temporal evolution of the flexible rod. Here $M = \text{diag}(\rho A, \rho A, \rho I)$ is the inertia matrix and ρ is the material density. We can then define the kinetic energy as

$$\mathcal{T} = \frac{1}{2} \int_0^{L_0} (\rho A ((\partial_t x)^2 + (\partial_t y)^2) + \rho I (\partial_t \theta)^2) ds$$

The Hamiltonian or the total energy of the system, $\mathcal{H}(q, p) = \mathcal{T}(p) + \mathcal{V}(q)$ can be utilized to equivalently write the free dynamics of a Cosserat rod as a Hamiltonian system with damping [17], [18]. The damping term serves to model the inherent viscoelasticity in the arm [15].

An octopus arm is actuated via internal muscle contractions. In this work, we assume there are N muscle actuators distributed along the length of the arm. The details of muscle modeling appear in the following section where the effect of the i -th actuator is shown to arise as a localized (but not pointwise, i.e. muscle actuation is distributed in nature) internal force and torque profile denoted as $G_i(q, p)$. It is assumed that the force generated by a muscle contraction is proportional to the intensity of contraction. By introducing $u_i(t) \in [0, 1]$ as a surrogate¹ for the intensity of contraction, the Hamiltonian control system is expressed as follows:

$$\begin{aligned} \frac{dq}{dt} &= \frac{\delta \mathcal{H}}{\delta p} \\ \frac{dp}{dt} &= -\frac{\delta \mathcal{H}}{\delta q} - \gamma M^{-1} p + \sum_{i=1}^N G_i(q, p) u_i(t) \end{aligned} \quad (5)$$

Equation (5) is accompanied by suitable boundary and initial conditions. At this stage, we make the following assumption on the functions G_i :

Assumption 1: The matrix $\hat{G}(q, p)$ defined as $\hat{G} := [g_{ij}]$, $g_{ij} = \langle G_i, G_j \rangle$, is invertible for all (q, p) . Here the inner product is taken in the usual L^2 sense.

Remark 1: This assumption is the continuum analogue of the full column rank assumption in the finite dimensional state space case [4], [5].

III. MUSCLE MODEL

A. Muscular organization in an octopus arm

The octopus arm is composed of a central axial nerve cord surrounded by densely packed muscle and connective tissues. Arm muscle tissues have three main orientations of fibers - (i) longitudinal, (ii) transverse, and (iii) oblique [8], [10]. Each of the three muscle groups serve a purpose in

the overall movement of the arm: the longitudinal muscles are responsible for shortening and bending, the transverse muscles are used to lengthen the arm and provide support in active bending, and the oblique ones produce torsion [9], [10]. A simplified 3D model depicting the muscular organization appears in Fig. 1a.

B. Modeling muscle actuation

In this paper, each of the N muscles is modeled to provide an internal distributed contraction force

$$n^m = n_1^m a + n_2^m b$$

and depending on the geometric muscular arrangement, it may also produce an internal couple on the center line of the arm itself

$$m^m = (r^m \times n^m) \cdot (e_1 \times e_2) = -r_2^m n_1^m + r_1^m n_2^m$$

where $r^m = r_1^m a + r_2^m b$ is the radial vector from the arm center line to the muscle (see Fig. 1c). This yields the following model for each of the N muscles:

$$G^m = \begin{bmatrix} \partial_s \left(\begin{pmatrix} \cos \theta & -\sin \theta \\ \sin \theta & \cos \theta \end{pmatrix} \begin{pmatrix} n_1^m \\ n_2^m \end{pmatrix} \right) \\ \partial_s m^m + \nu_1 n_2^m - \nu_2 n_1^m \end{bmatrix} \quad (6)$$

where the superscript m denotes muscle and is later replaced by different muscle type such as longitudinal muscle (LM) and transverse muscle (TM).

It remains to prescribe a model for the contraction force n^m . This force is known to be comprised of active and passive parts. Passive forces are due to the non-contracting parts of the muscle and is also attributed to its elastic response. This force has a typical non-linear stress-strain response that has not yet been fully characterized in octopuses. In this paper, we make the following simplifying assumption:

Assumption 2: We ignore the passive component of the muscle forces, rather the overall passive elastic internal forces and couples (an aggregate effect of muscle fibers, axial nerve cord, and arm tissue) are assumed to follow the linear stress-strain relationship as described in Sec. II-A.

Remark 2: The above assumption might appear as a considerable simplification of the actual mechanics. However, an earlier numerical study [14] found no significant drawback of the linear model, albeit in a discretized crude arm model.

The active force component is generated by the overlapping actin-myosin chains. The magnitude of the force depends on the length and velocity of the muscle fiber. The muscle length is determined by its stretch strain, denoted as ν^m , which is a function of the deformation of the rod w . Muscle velocity is denoted by $\dot{\nu}^m$ which is simply the time derivative of ν^m . We use the functions $F_l(\cdot)$ and $F_v(\cdot)$ to capture the force-length and force-velocity relationships, respectively. These are modeled after the Hill's muscle model [13], details of which appear in Appendix I.

When a muscle is activated by a neuronal stimulation at a point $s = s_0$, the magnitude of the contraction force is experimentally observed to be distributed along the length s

¹Physically, the control $u_i(t)$ may be related to the neuronal stimulation, such as the firing frequency of the motor neuron innervating the muscle.

with the maximum at the point of activation. We model this with a Gaussian function centered at $s = s_0$. This, together with the Hill's model, yields the following formula for the magnitude of a muscle contraction force:

$$n_{\text{mag}}^m(s, \nu^m, \dot{\nu}^m; s_0) = A^m(s) n_{\text{max}}^m F_l(\nu^m) F_v(\dot{\nu}^m) e^{-\frac{1}{2} \left(\frac{s-s_0}{\sigma_a^m} \right)^2} \quad (7)$$

where A^m is a fraction of the arm cross sectional area occupied by the muscle, n_{max}^m is the maximum producible force per unit area, the parameter σ_a^m captures the spatial extent of the activation to that muscle.

We are now able to completely specify the model for the contractive force n^m :

1) *Longitudinal muscles*: Longitudinal muscles are long muscles that run along the length of the arm parallel to the center line (see Fig. 1a,c). In the planar case we consider them positioned at a distance $\phi^{\text{LM}}(s)$ away from the center line. Hence the position vector of a longitudinal muscle is given as $r + r^m$, where $r^m = \pm \phi^{\text{LM}} \mathbf{b}$ where the sign depends on the side of the center line the LM is located. Taking spatial derivative of the muscle position, we deduce that the local stretch strain is given by $\nu^m = \nu_1 \mp \phi^{\text{LM}} \kappa$. When a longitudinal muscle is activated, it only generates contraction force along the longitudinal direction \mathbf{a} , i.e., $n^m = n_{\text{mag}}^{\text{LM}} \mathbf{a}$, and since it acts at a distance away from the center line, it also produces a couple $m^m = \mp \phi^{\text{LM}} n_{\text{mag}}^{\text{LM}}$ which serves to bend the arm locally.

2) *Transverse muscles*: Transverse muscles surround the axial nerve cord, which means $r^m = 0$. When a transverse muscle contracts, it creates a pressure that squeezes the nerve cord, lowering the cross-sectional area locally. Owing to the constancy of volume, the arm extends. Such a behavior is modeled by letting an extension distributed force act along the $-\mathbf{a}$ direction, i.e., $n^m = -n_{\text{mag}}^{\text{TM}} \mathbf{a}$. The local stretch strain is modeled as $\nu^m = \frac{1}{\sqrt{\nu_1^2 + \nu_2^2}}$, which is the ratio of the diameter of the cross section to the one at rest.

IV. ENERGY SHAPING CONTROL DESIGN

The key idea of the energy shaping control scheme is to implement a control $u(t)$ such that Hamiltonian is modified from $\mathcal{H} = \mathcal{T} + \mathcal{V}$ to $\mathcal{H}^d = \mathcal{T} + \mathcal{V}^d$. That is, the controlled system evolves according to

$$\begin{aligned} \frac{dq}{dt} &= M^{-1} p \\ \frac{dp}{dt} &= -\frac{\delta \mathcal{V}^d}{\delta q} - \gamma M^{-1} p \end{aligned} \quad (8)$$

For the two systems (5) and (8) to exactly 'match' (for arbitrary choice of initial conditions), it must follow that

$$\sum_{i=1}^N G_i(q, p) u_i = \frac{\delta \mathcal{V}}{\delta q} - \frac{\delta \mathcal{V}^d}{\delta q}, \quad \forall (q, p) \quad (9)$$

This restricts the selection of desired potential energy \mathcal{V}^d , which is the main difference with the no-muscle constraint case where \mathcal{V}^d can be arbitrarily designed. The restriction

on \mathcal{V}^d is expressed in the form of the matching condition which is described next.

Let $G^\perp(q, p)$ denote the annihilator of $G_i(q, p)$, i.e., $\langle G^\perp, G_i \rangle = 0$, $i = 1, \dots, N$ and for all (q, p) . Then applying G^\perp to both sides of (9), we get

$$\left\langle G^\perp, \left(\frac{\delta \mathcal{V}}{\delta q} - \frac{\delta \mathcal{V}^d}{\delta q} \right) \right\rangle = 0, \quad \forall (q, p) \quad (10)$$

Equation (10) is referred to as the (potential) *matching condition* [4]–[6], [19]. Its general solution expresses the set of allowable \mathcal{V}^d that may be used in the energy shaping control design. For example, in the fully actuated case without explicit muscle constraints, $G^\perp = 0$, so any choice of \mathcal{V}^d is a solution. Even in the finite dimensional settings, it is a challenging task to solve the matching condition PDEs for \mathcal{V}^d . Such settings typically require specialized techniques, e.g. the λ -method [7], or additional assumptions on the system dynamics and actuator modeling [6], [20].

A. Design of potential energy: The static problem

We begin by recalling the optimization problem (4) which is used to model the control objective.

In this paper, we consider only the quadratic form (3) of the potential energy whereby \mathcal{V}^d is parameterized by the (static) deformation w^d . In fully actuated settings, the optimization problem (4) is solved to obtain the desired (static) deformation w^d . Clearly, in the presence of muscle constraints, the choice of allowable deformations is restricted (as dictated by the matching condition). The following proposition gives a formula for static deformation as a solution of a nonlinear equation.

Proposition 4.1: Consider a quadratic form (3) of the potential energy \mathcal{V}^d . Then the control system (5) and the desired system (8) have the same equilibrium if the deformation $w^d(s) = (\nu_1^d(s), \nu_2^d(s), \kappa^d(s))$ satisfy

$$\begin{bmatrix} EA(\nu_1^d(s) - 1) \\ GA\nu_2^d(s) \\ EI\kappa^d(s) \end{bmatrix} = - \begin{bmatrix} \sum \alpha_i n_{\text{mag}}^{m,i}(s, w^d(s)) \\ 0 \\ \sum \alpha_i m^{m,i}(s, w^d(s)) \end{bmatrix}, \quad \forall s \in [0, L_0] \quad (11)$$

where $\alpha = (\alpha_1, \dots, \alpha_N) \in [0, 1]^N$ and $u_i = \alpha_i$.

Proof: With $u_i = \alpha_i$, the matching condition (9) at the equilibrium is expressed as

$$\frac{\delta \mathcal{V}}{\delta q} - \frac{\delta \mathcal{V}^d}{\delta q} = \sum_{i=1}^N G_i(q, 0) \alpha_i \quad (12)$$

Using the formulae of \mathcal{V} and \mathcal{V}^d in (12)

$$\begin{aligned} & \left[\partial_s \left(\begin{pmatrix} \cos \theta & -\sin \theta \\ \sin \theta & \cos \theta \end{pmatrix} \begin{pmatrix} EA(\nu_1^d(s) - 1) \\ GA\nu_2^d(s) \end{pmatrix} \right) \right] \\ & \left[\partial_s (EI\kappa^d(s)) + \nu_1 GA\nu_2^d(s) - \nu_2 EA(\nu_1^d(s) - 1) \right] \\ & = - \left[\partial_s \left(\begin{pmatrix} \cos \theta & -\sin \theta \\ \sin \theta & \cos \theta \end{pmatrix} \begin{pmatrix} \sum \alpha_i n_{\text{mag}}^{m,i}(s, w^d(s)) \\ 0 \end{pmatrix} \right) \right] \\ & \left[\partial_s (\sum \alpha_i m^{m,i}(s, w^d(s))) - \nu_2 (\sum \alpha_i n_{\text{mag}}^{m,i}(s, w^d(s))) \right] \end{aligned} \quad (13)$$

at $q = q^d$ (defined according to $\partial_s q^d = f(q^d, w^d)$ with $q^d(0) = q_0$). It is straightforward to verify that (13) holds if (11) is satisfied. ■

For a given $\alpha \in [0, 1]^N$, the solution of (11) is denoted as $w^d(s; \alpha)$. To obtain the desired deformation, the following optimization problem is considered:

$$\begin{aligned} & \underset{\alpha \in [0, 1]^N}{\text{minimize}} \quad J(\alpha) = \int_0^1 W(w^d) + \mu_{\text{grasp}}(s) \Phi_{\text{grasp}}(q^d) \, ds \\ & \quad + \mu_{\text{tip}} \Phi_{\text{tip}}(q^d(L_0), q^*) \\ & \text{subject to} \quad \Psi_j(q^d) \leq 0, \quad j = 1, 2, \dots, N_{\text{obs}}; \\ & \quad \text{and} \quad \partial_s q^d = f(q^d, w^d), \text{ with } q^d(0) = q_0; \\ & \quad \text{and} \quad w^d = w^d(\cdot; \alpha) \end{aligned} \quad (14)$$

The problem (14) is similar to (4) except that the optimization is carried out over the deformations which satisfy the matching condition by construction. The solution w^d of the optimization problem (14) is used to define the desired energy \mathcal{V}^d via the quadratic form (3).

Remark 3: It must be noted that although we have designed a candidate potential energy \mathcal{V}^d , it is in general *not* a solution to the matching condition (10). The condition is guaranteed to be satisfied only at the equilibrium.

B. Energy shaping control law

We seek a control input $u = u(t)$ such that along the controlled trajectory

$$\sum_{i=1}^N G_i(q(t), p(t)) u_i(t) = \frac{\delta \mathcal{V}}{\delta q}(q(t)) - \frac{\delta \mathcal{V}^d}{\delta q}(q(t)), \quad \forall t \geq 0$$

Since \mathcal{V}^d is not necessarily a solution of the matching condition (10), there may not exist a solution $u(t)$ for this problem. It is natural to therefore introduce an error

$$e(t) := \sum_{i=1}^N G_i(q(t), p(t)) u_i(t) - \left(\frac{\delta \mathcal{V}}{\delta q}(q(t)) - \frac{\delta \mathcal{V}^d}{\delta q}(q(t)) \right) \quad (15)$$

and choose $u(t)$ to minimize $\|e(t)\|_{L^2}$ (pointwise in time). If the controls are not constrained to be bounded between 0 and 1, the solution to this problem is easily obtained by the least-square formula

$$u(t) = \hat{G}(q(t), p(t))^{-1} z(t) \quad (16)$$

where $u(t) = [u_1(t), \dots, u_N(t)]^T$, $z(t) = [z_1(t), \dots, z_N(t)]^T$, and $z_i(t) := \left\langle G_i(q(t), p(t)), \left(\frac{\delta \mathcal{V}}{\delta q}(q(t)) - \frac{\delta \mathcal{V}^d}{\delta q}(q(t)) \right) \right\rangle$. It is easy to see that if \mathcal{V}^d satisfies the matching condition then the error is zero. In fact, the control law (16) is widely used in finite-dimensional settings [4], [5]. Since the controls are bounded in our model, we solve the bounded variable least squares problem

$$\underset{u(t) \in [0, 1]^N}{\text{minimize}} \quad \|e(t)\|_{L^2} \quad (17)$$

At this point, it is worthwhile to mention the special case where the Hill's model is ignored by assuming $F_l(\nu^m) \equiv 1$ and $F_v(\dot{\nu}^m) \equiv 1$. In this case, the muscle contractile forces n_{mag}^m and couples m^m are functions of s only (see (7)),

TABLE I: Parameters

Parameter	Description	Value
Numerical Simulation		
L_0	rest arm length [cm]	20
ϕ_{base}	base radius [cm]	1.2
ϕ_{tip}	tip radius [cm]	0.1
E	Young's modulus [kPa]	10
G	Shear modulus [kPa]	20/3
ρ	density [kg/m ³]	700
γ	dissipation [kg/s]	0.02
N_d	discrete number of elements	100
Δt	discrete time-step [s]	10^{-5}
Hill's Muscle Model		
ν^{rest}	rest stretch creating maximum force	1
σ	range of strain creating force	0.2
$\dot{\nu}^{\text{max}}$	maximum stretch rate	300
Muscle Architecture		
s_0/L_0	center positions of muscles	[0.2, 0.4, 0.6, 0.8]
$\text{LM}_l \text{ LM}_b$	Longitudinal Muscle Groups	
$n_{\text{mag}}^{\text{LM}}$	maximum force per unit area	1
$\phi^{\text{LM}}(s)$	off center distance	$2\phi(s)/3$
σ_a^{LM}	effective range of each muscle	$0.05 L_0$
TM	Transverse Muscle Group	
$n_{\text{mag}}^{\text{TM}}$	maximum force per unit area	1.5
σ_a^{TM}	effective range of each muscle	$0.025 L_0$

and the solution of the matching condition simplifies considerably. This simplification is described in the following proposition:

Proposition 4.2: Consider the control system (5) with $F_l(\nu^m) \equiv 1$ and $F_v(\dot{\nu}^m) \equiv 1$. Let $\alpha \in [0, 1]^N$ be any constant vector. Then

(i) The potential energy \mathcal{V}^d parametrized by solution w^d of the nonlinear equation

$$\begin{bmatrix} EA(\nu_1^d(s) - 1) \\ GA\nu_2^d(s) \\ EI\kappa^d(s) \end{bmatrix} = - \begin{bmatrix} \sum \alpha_i n_{\text{mag}}^{m,i}(s) \\ 0 \\ \sum \alpha_i m^{m,i}(s) \end{bmatrix} \quad \forall s \in [0, L_0] \quad (18)$$

solves the matching condition (10).

(ii) Along the closed-loop trajectory, the error $e(t) \equiv 0$, and the control $u(t) \equiv \alpha$ is constant.

Proof: We start by noticing that in this case, $G(q, p) \equiv G(q, 0)$ for all (q, p) .

(i) A solution to the matching condition (10) is given by equation (12) that needs to be satisfied for all (q, p) , where $\alpha \in [0, 1]^N$ is some constant vector. Plugging the formulae of \mathcal{V} and \mathcal{V}^d in (12) leads to (13), where on the right hand side the muscle force and couple terms are now w^d independent. It is immediate that the choice (18) of w^d satisfies (13) for all (q, p) , not only at the equilibrium.

(ii) Since in this case the matching condition holds for all (q, p) , by the definition of $z(t)$ we calculate $z(t) = \hat{G}(q(t), 0)\alpha$. Then, the controls $u(t) = \alpha$ are constant in time, which follows directly from (17). ■

V. NUMERICAL SIMULATION

In this section, we describe the numerical environment used to simulate the soft octopus arm. We use two nu-

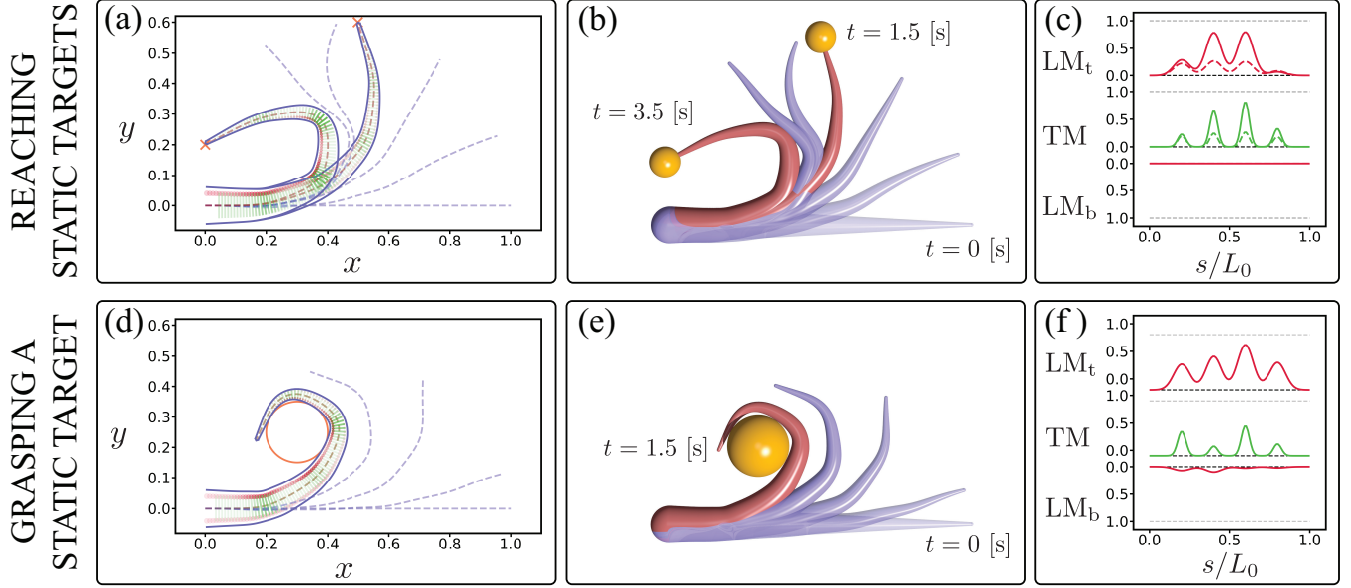


Fig. 2: Arm reaching and grasping control tasks. (a-c) An arm is tasked to reach two different locations one after the other. Octopuses use this type of motion to fetch a food source, a shrimp for example, and then bring it back to the mouth. (a) Targets are located at $r^* = (10, 12)$ and $(0, 4)$ [cm] (axes normalized by undeformed arm length L_0) and indicated as orange crosses. The dashed purple lines indicate the transient response and the solid ones show the arm when it reaches each target. The transparency of the green and red color represents how much each muscle is activated. The red ones on both sides indicate the longitudinal muscles and the green one in the middle indicates the transverse muscle. (b) Arm front view: Targets are represented as small orange spheres. Terminal arm configurations are depicted in reddish-brown color, while the transient arm motion is depicted in purple. (c) This shows the activation profile of each muscle. (horizontal axis is normalized by L_0 .) The rows represent the muscle groups: the top side longitudinal muscle, the transverse muscle in the middle, and the bottom side longitudinal muscle. Dashed lines represent the activation for the first target, and solid ones represent the activation for the second target. (d-f) An arm is tasked to wrap around a static sphere of diameter 4 [cm] and centered at $(6, 5)$ [cm]. The color codes are the same as in (a-c).

merical experiments to demonstrate our capabilities of the muscle control approach. The simulations include octopus arm reaching and grasping motions.

A. Arm discretization and muscle architecture

The explicit dynamic equations of motion of a planar Cosserat rod [17] are as follows:

$$\begin{aligned} \partial_t(\rho A \partial_t r) &= \partial_s n + F \\ \partial_t(\rho I \partial_t \theta) &= \partial_s m + \nu_1 n_1 - \nu_2 n_1 + C \end{aligned} \quad (19)$$

where $n = n_1 a + n_2 b$ and m are rod internal forces and couple, respectively. The external forces and couple per unit length here are taken as the controls term $\sum G_i u_i$. The rod starts in the undeformed straight initial condition (20) and satisfies the fixed base and free tip boundary conditions (21) for $t \geq 0$.

$$r(s, 0) = r^\circ(s), \quad \theta(s, 0) = 0, \quad \partial_t r(s, 0) = 0, \quad \partial_t \theta(s, 0) = 0 \quad (20)$$

$$r(0, t) = 0, \quad \theta(0, t) = 0, \quad n(L_0, t) = 0, \quad m(L_0, t) = 0 \quad (21)$$

where $r^\circ(s) = (s, 0)$ is the initial position vector. These governing equations of the Cosserat rod theory are discretized into N_d connected cylindrical segments and solved numerically by using our open-source, dynamic, three-dimensional simulation framework *Elastica* [15].

To model the tapered geometry of an octopus arm, the radius profile of the arm is varied as follow:

$$\phi(s) = \phi_{\text{tip}} s + \phi_{\text{base}}(L_0 - s).$$

The cross sectional area and the second moment of area are calculated as $A = \pi \phi^2$ and $I = \frac{A^2}{4\pi}$. The parameter values in this work are listed in Table I and also in reference [18].

The muscle architecture along the arm can be characterized as two longitudinal muscle groups on both sides (LM_t and LM_b denoting the top one and the bottom one, respectively, see Fig. 1c) and one transverse muscle group at the center (TM). In each group, there are four muscles centered at s_0/L_0 as listed in Table I. For LM_t , LM_b , they are located at ϕ^{LM_b} , $-\phi^{LM_b}$ away from the center line, respectively. Each muscle can produce n_{max}^{LM} maximum magnitude of contraction force with spatial extent parameter σ_a^{LM} . For the TM, each of them can provide extension force with maximum magnitude of n_{max}^{TM} and has spatial extent parameter σ_a^{TM} .

B. Experiments

Two experiments, including reaching and grasping tasks, are presented in this section. Solving any task involves two steps. The first step is to find the static configuration by

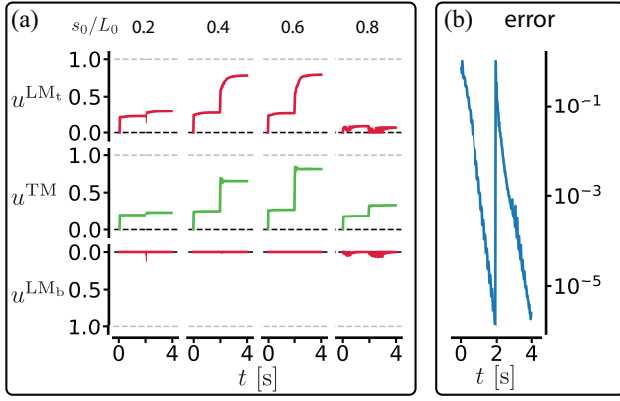


Fig. 3: The control and error plots for the reaching experiment. The change of the target position at time $t = 2$ [s] is reflected by the jumps at all the graphs. (a) The control of each muscle $u_i(t)$ is calculated by solving the minimization problem (17) at each t . (b) This plot shows the time trajectory of the norm of the error (15). The error is normalized by its initial value. Both error trajectories decay over time.

solving (14) offline; and the second step is to use (17) to obtain the muscle control time sequence. The minimization problem (14) is solved by using the sequential least square programming method (*SLSQP*) in the *scipy* package to obtain the optimal α . In order to calculate the cost corresponding to each α , the strains w^d are required to be computed from the nonlinear equations (11) pointwise in the arc-length parameter s . In our experiments, we utilize the *fsolve* routine in the *scipy* package to solve (11) for w^d . Once the desired static equilibrium is found, the energy shaping control inputs are calculated as the minimizer of the problem (17) at each time. The minimization problem (17) is solved numerically by the quadratic programming algorithm *qpsovers 1.4* in *scipy*.

1) *Reaching multiple static targets*: The first experiment consists of tasks to reach multiple targets one by one to mimic the behavior of a real octopus. For any target, the tip cost function Φ_{tip} in (14) is set as

$$\Phi_{\text{tip}}(q(L_0), r^*) = \frac{1}{2} |r^* - r(L_0)|^2 \quad (22)$$

The cost does not depend on the tip angle $\theta(L_0)$ as we are not concerned about the tip pose. The weight function μ_{grasp} is chosen to be zero and regularization parameter μ_{tip} is set as 10^5 . Simulation results are shown in Fig. 2a-c. Target positions are given as r^* , illustrated as small orange spheres. Results show that the tip of the arm reach each target one after another. The control and error time trajectories are shown in Fig. 3.

2) *Grasping an object*: In the second experiment, the *CyberOctopus*' arm is tasked to grasp a target ball. This behavior is commonly seen when an octopus is trying to reach for a bottle, a shell or a crab. To find the desired static configuration via (14), the object is treated as an obstacle so that the arm cannot penetrate it. The inequality constraint

model of it is:

$$\Psi(q(s)) = (\phi^{\text{obj}} + \phi(s))^2 - |r^{\text{obj}} - r(s)|^2$$

where ϕ^{obj} and r^{obj} denote the radius and center position of the object, respectively. In addition, since we want the arm to grasp the target ball, the running cost Φ_{grasp} in (14) is designed so that the arm can get as close to the boundary as possible:

$$\Phi_{\text{grasp}}(q(s)) = \text{dist}(\Omega, r(s))$$

where Ω denotes the boundary of the object (here just a circle) and $\text{dist}(\cdot, \cdot)$ calculates the distance between the boundary and the point $r(s)$. We also choose the following weight function

$$\mu_{\text{grasp}}(s) = 10^5 \chi_{[0.4L_0, L_0]}(s)$$

where $\chi_{[s_1, s_2]}(\cdot)$ denotes the characteristic function of $[s_1, s_2]$. Such a design together with the inequality constraint cause the distal portion of the arm, starting from $s = 0.4L_0$, to grasp the target ball without penetrating it. The value of μ_{tip} is 0 in this case. Fig. 2d-f shows the simulation results where the arm tries to grasp the ball under its actuation constraints.

VI. CONCLUSION AND FUTURE WORK

In this paper, a flexible octopus arm is represented as a planar Cosserat rod and its muscle mechanisms are modeled as distributed internal force/couple functions with the activation as the control inputs. The rod is viewed as an underactuated Hamiltonian control system, for which an energy shaping control method is sought to solve various manipulation objectives, e.g. reaching and grasping. We have shown that a solution to the matching conditions yields a finite dimensional optimization problem whose solution generates the desired deformed equilibrium configuration. The energy shaping control inputs are then found by solving a bounded variable least squares problem. Numerical experiments are demonstrated to present the efficacy of this scheme. As a direct extension, a more sophisticated muscle actuation model and the corresponding control method can be applied to the general 3D case. Another direction of future work is to develop an octopus-inspired sensorimotor control system where only a part of the state is available to the controller through internal distributed sensors.

REFERENCES

- [1] D. Rus and M. T. Tolley, "Design, fabrication and control of soft robots," *Nature*, vol. 521, no. 7553, pp. 467–475, 2015.
- [2] G. Singh and G. Krishnan, "A constrained maximization formulation to analyze deformation of fiber reinforced elastomeric actuators," *Smart Materials and Structures*, vol. 26, no. 6, p. 065024, 2017.
- [3] C. Della Santina, R. K. Katzschmann *et al.*, "Dynamic control of soft robots interacting with the environment," in *2018 IEEE International Conference on Soft Robotics (RoboSoft)*. IEEE, 2018, pp. 46–53.
- [4] R. Ortega, M. W. Spong *et al.*, "Stabilization of a class of underactuated mechanical systems via interconnection and damping assignment," *IEEE transactions on automatic control*, vol. 47, no. 8, pp. 1218–1233, 2002.
- [5] G. Blankenstein, R. Ortega, and A. J. Van Der Schaft, "The matching conditions of controlled lagrangians and ida-passivity based control," *International Journal of Control*, vol. 75, no. 9, pp. 645–665, 2002.

- [6] A. M. Bloch, N. E. Leonard, and J. E. Marsden, “Controlled lagrangians and the stabilization of mechanical systems. i. the first matching theorem,” *IEEE Transactions on automatic control*, vol. 45, no. 12, pp. 2253–2270, 2000.
- [7] D. Auckly, L. Kapitanski, and W. White, “Control of nonlinear underactuated systems,” *Communications on Pure and Applied Mathematics: A Journal Issued by the Courant Institute of Mathematical Sciences*, vol. 53, no. 3, pp. 354–369, 2000.
- [8] W. M. Kier and M. P. Stella, “The arrangement and function of octopus arm musculature and connective tissue,” *Journal of Morphology*, vol. 268, no. 10, pp. 831–843, 2007.
- [9] N. Feinstein, N. Neshet, and B. Hochner, “Functional morphology of the neuromuscular system of the octopus vulgaris arm,” *Vie et milieu (1980)*, vol. 61, no. 4, pp. 219–229, 2011.
- [10] W. M. Kier, “The musculature of coleoid cephalopod arms and tentacles,” *Frontiers in cell and developmental biology*, vol. 4, p. 10, 2016.
- [11] G. Levy, N. Neshet *et al.*, “Motor control in soft-bodied animals: the octopus,” in *The Oxford Handbook of Invertebrate Neurobiology*, 2017.
- [12] N. Neshet, F. Maiolo *et al.*, “From synaptic input to muscle contraction: arm muscle cells of octopus vulgaris show unique neuromuscular junction and excitation–contraction coupling properties,” *Proceedings of the Royal Society B*, vol. 286, no. 1909, p. 20191278, 2019.
- [13] A. V. Hill, “The heat of shortening and the dynamic constants of muscle,” *Proceedings of the Royal Society of London. Series B-Biological Sciences*, vol. 126, no. 843, pp. 136–195, 1938.
- [14] Y. Yekutieli, R. Sagiv-Zohar *et al.*, “Dynamic model of the octopus arm. i. biomechanics of the octopus reaching movement,” *Journal of neurophysiology*, vol. 94, no. 2, pp. 1443–1458, 2005.
- [15] M. Gazzola, L. Dudte *et al.*, “Forward and inverse problems in the mechanics of soft filaments,” *Royal Society Open Science*, vol. 5, no. 6, p. 171628, 2018.
- [16] X. Zhang, F. K. Chan *et al.*, “Modeling and simulation of complex dynamic musculoskeletal architectures,” *Nature Communications*, vol. 10, no. 1, pp. 1–12, 2019.
- [17] S. S. Antman, *Nonlinear Problems of Elasticity*. Springer, 1995.
- [18] H.-S. Chang, U. Halder *et al.*, “Energy shaping control of a cyberoctopus soft arm,” *arXiv preprint arXiv:2004.05747*, 2020.
- [19] R. Ortega, A. Van Der Schaft *et al.*, “Interconnection and damping assignment passivity-based control of port-controlled hamiltonian systems,” *Automatica*, vol. 38, no. 4, pp. 585–596, 2002.
- [20] F. Gomez-Estern, R. Ortega *et al.*, “Stabilization of a class of under-actuated mechanical systems via total energy shaping,” in *Proceedings of the 40th IEEE Conference on Decision and Control (Cat. No. 01CH37228)*, vol. 2. IEEE, 2001, pp. 1137–1143.
- [21] F. E. Zajac, “Muscle and tendon: properties, models, scaling, and application to biomechanics and motor control,” *Critical reviews in biomedical engineering*, vol. 17, no. 4, pp. 359–411, 1989.

APPENDIX I HILL’S MODEL

Due to the overlap of actin and myosin filaments in muscle, the amount of tension that can be developed by a muscle fiber is dependent on the amount of overlap between the actin and myosin filaments, known as the force-length relationship. The force generated by a muscle fiber typically shows a bell shaped dependence on the muscle length. In the rest length of the muscle, where the actin and myosin filaments are not moving past each other, it generates the maximum possible tension. Additionally, the active force exhibits a fiber velocity dependence. If a fiber is rapidly contracting, the actin-myosin connections are rapidly shortening and so are unable to generate their maximum amount of tension. The combination of these two effects leads to a force-length-velocity relationship that is known as the Hill’s model. Let ν^m denote the muscle stretch strain and $\dot{\nu}^m$ is its time derivative. We consider the force-length

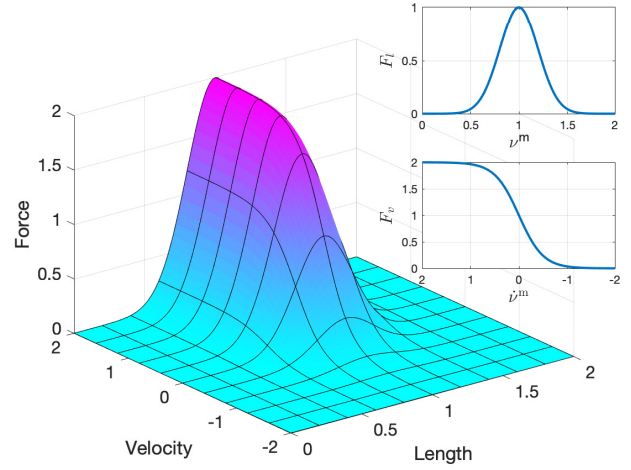


Fig. 4: Force-length-velocity relationship for muscles as described in the Hill’s model (length and velocity axes are normalized). Force-length and force-velocity curves are also shown in the inset.

and force-velocity relationships as

$$F_l(\nu^m) = \exp\left(-\frac{1}{2}\left(\frac{\nu^m - \nu^{\text{rest}}}{\sigma}\right)^2\right) \quad (\text{A-1})$$

$$F_v(\dot{\nu}^m) = 1 + \tanh\left(\frac{\dot{\nu}^m}{\dot{\nu}^{\text{max}}}\right) \quad (\text{A-2})$$

where the design parameters are: ν^{rest} is the rest strain of the muscle that can produce the maximum magnitude of force and σ controls the range of strain that can generate muscle force, $\dot{\nu}^{\text{max}}$ determines the maximum contraction speed at which the force generation ceases. A representative force-length-velocity relationship is shown in Fig. 4.

Remark 4: The functions (A-1)-(A-2) are motivated from skeletal muscle models [21], which have also been used in octopus arm muscle modeling [14]. There is nothing special about the functional form used in this paper. An ongoing experimental work aims to obtain the force-length-velocity relationship of octopus arm muscles.